

A Hybrid-Potential Free-Energy Study of the Isomerization Step of the Acetohydroxy Acid Isomeroreductase Reaction

Flavien Proust-De Martin,[†] Renaud Dumas,[‡] and Martin J. Field^{*,†}

Contribution from the Laboratoire de Dynamique Moléculaire, Institut de Biologie Structurale, Jean-Pierre Ebel 41, rue Jules Horowitz, F-38027 Grenoble Cedex 01, France, and Unité Mixte CNRS/Aventis Crop Science (UMR 1932), 14-20, rue Pierre Baizet, 69263 Lyon Cedex 09, France

Received February 3, 2000

Abstract: The enzyme acetohydroxy acid isomeroreductase is a promising target for the design of herbicides because it is an essential enzyme for the synthesis of branched-chain amino acids in plants but is absent in animals. In this paper, we examine with theoretical simulation techniques one hypothesis for the mechanism of the purported rate-limiting step in the reaction catalyzed by the enzyme—namely, the isomerization of the deprotonated substrate which involves the migration of a methyl or ethyl group from one carbon to its neighbor. To determine the free-energy profiles for the reaction we used a hybrid semiempirical quantum mechanical/molecular mechanical (QM/MM) potential in conjunction with potential of mean force calculations. To obtain accurate results we found it necessary to correct the semiempirical QM method with a term derived from calculations performed with more precise ab initio quantum chemical methods. For the mechanism we studied, our simulations predict that the isomerization occurs simultaneously with a proton transfer to the substrate from a protonated glutamate residue of the protein.

1. Introduction

Acetohydroxy acid isomeroreductase (AHIR; EC 1.1.1.86) is an enzyme involved in the biosynthetic pathway of branched-chain amino acids where it catalyzes the transformation of 2-aceto-lactate (AL) or 2-aceto-2-hydroxybutyrate (AHB) into 2,3-dihydroxy-3-isovalerate (DHIV) or 2,3-dihydroxy-3-methylvalerate (DHMV) (see Figure 1). Because the pathway of which AHIR forms a part occurs in plants and microorganisms but is absent in animals, AHIR is a promising target for inhibition by substances which selectively target these organisms, such as herbicides. Preliminary studies have revealed two inhibitors, 2-dimethylphosphinoyl-2-hydroxyacetic acid (HOE 704) and *N*-hydroxy-*N*-isopropylloxamate (IpOHA),^{1,2} but they show poor herbicidal action since these compounds are competitive inhibitors that bind very slowly to the enzyme.³

The AHIR reaction proceeds in two steps. First, there is an isomerization reaction that consists of an alkyl migration between carbon C2 and carbon C3 of the substrate and gives 3-hydroxy-2-oxo-isovalerate (HOIV) or 3-hydroxy-3-methyl-2-oxo-isovalerate (HMOV) (see Figure 1). Second, these intermediates are transformed by an NADPH-dependent reduction of the ketone moiety to give the final product. Both steps require the presence of magnesium cations in the active site of the enzyme, and Dumas et al. have demonstrated that two different magnesiums are involved in each part of the reaction.⁴ In the same paper, a reaction mechanism for AHIR was also proposed (see Figure 2). It was suggested that a protein base or

a hydroxyl coordinated to a magnesium abstracts the proton of the substrate's hydroxyl group. The alkyl group then migrates from the C2 carbon to the C3 carbon facilitated by the magnesium-induced polarization of the ketone group. Finally, the hydride transfer occurs, but this time the second magnesium enhances the reaction by the induction of a partial positive charge on the C2 carbon.

After publication of the work of Dumas et al., a crystallographic structure of AHIR complexed with NADPH, magnesium cations, and IpOHA was obtained by Biou et al. at a resolution of 1.65 Å.⁵ The structure showed that there are two magnesium ions in the active site—one of them, MgI, bound to region III of the protein via two residues, Asp 315 and Glu 319, and the other, MgII, bound directly to Asp 315 and indirectly to residues Glu 492 and Glu 496 of region IV of the protein via hydrogen-bonded water.

This paper describes an investigation of a possible mechanism for the isomerization step of the AHIR reaction (step b in Figure 2) using theoretical simulation methods. The aim of the work has been to obtain an understanding of which residues of the enzyme are important for catalysis of the reaction and then to use this information in the design of more effective competitive inhibitors that block the protein's action. All the results in this paper are for the AHB form of the substrate because this is the substrate for which the enzyme is most active, but we have done a more limited study with the AL substrate and obtain very similar behavior.

The outline of this paper is as follows. Section 2 details the theoretical procedures that we used to simulate the reaction, section 3 presents and discusses the results of our simulations, and section 4 concludes the paper.

(5) Biou, V.; Dumas, R.; Cohen-Addad, C.; Douce, R.; Job, D.; Pebay-Peyroula, E. *EMBO J.* **1997**, *16*, 3405–3415.

[†] Laboratoire de Dynamique Moléculaire, Institut de Biologie Structurale.

[‡] Unité Mixte CNRS/Aventis Crop Science.

(1) Schulz, A.; Spönmann, P.; Köcher, H.; Wengenmayer, F. *FEBS Lett.* **1988**, *238*, 375–378.

(2) Aulabaugh, A.; Schloss, J. V. *Biochemistry* **1990**, *29*, 2824–2830.

(3) Dumas, R.; Cornillon-Bertrand, C.; Guigue-Talet, P.; Genix, P.; Douce, R.; Job, D. *Biochem. J.* **1994**, *301*, 813–820.

(4) Dumas, R.; Butikofer, M. C.; Job, D.; Douce, R. *Biochemistry* **1995**, *34*, 6026–6036.

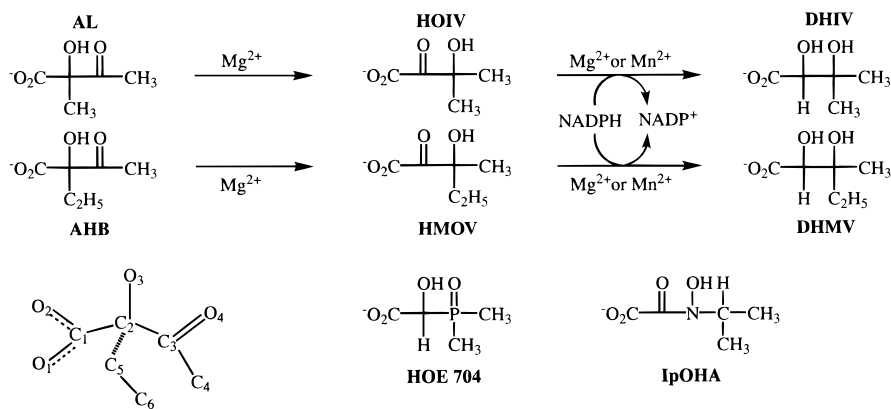


Figure 1. Schematic diagram of the reactions catalyzed by AHIR and the structures of the substrate AHB (with atom numbering) and the selective inhibitors IpOHA and HOE 704. Abbreviations: AHB, 2-aceto-2-hydroxybutyrate; AL, 2-acetolactate; DHIV, 2,3-dihydroxy-3-isovalerate; DHMV, 2,3-dihydroxy-3-methylvalerate; HOIV, 3-hydroxy-2-oxo-isovalerate; HMOV, 3-hydroxy-3-methyl-2-oxo-isovalerate.

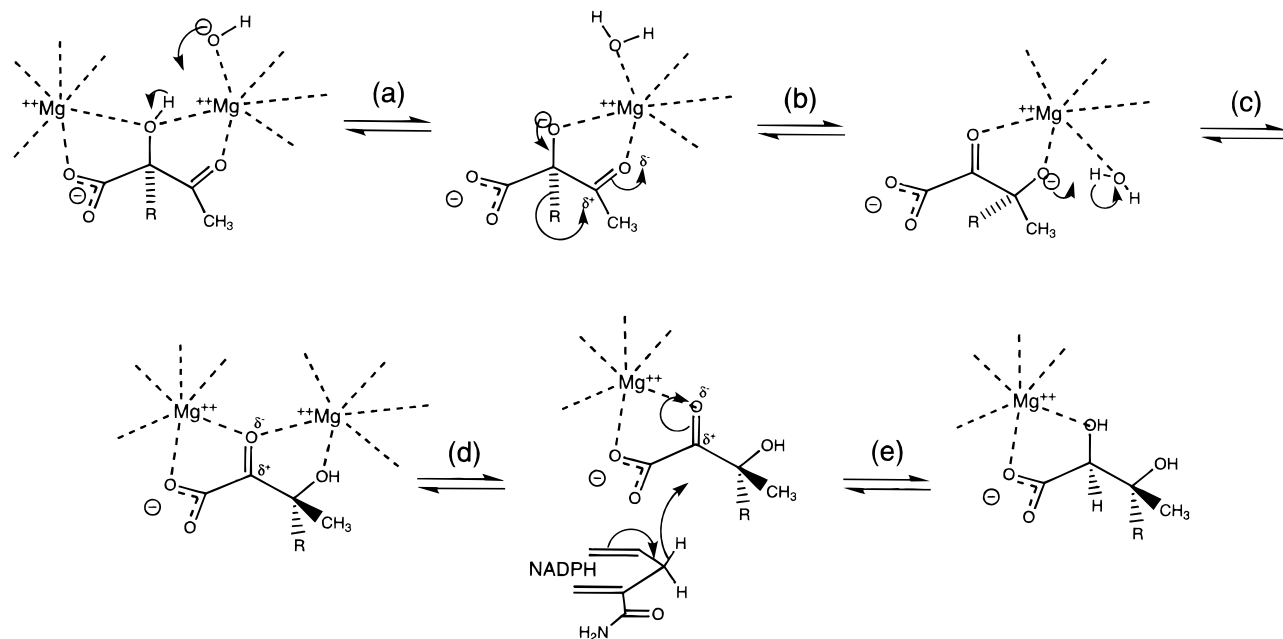


Figure 2. Proposed mechanism of reaction for AHIR.

2. Methods

The simulation of enzymatic or other condensed-phase reactions presents a challenge for theoretical techniques. The natural tools to use when studying reactions are quantum chemical ones, but these are computationally expensive and cannot be applied to systems the size of proteins. To overcome this limitation a range of other techniques have been developed. One of the most successful of these is the hybrid potential method in which a quantum mechanical (QM) potential is used to model the small region of the system in which the reaction is occurring and a simpler molecular mechanical (MM) force field is employed for the remainder of the atoms which act as an environment to the QM region.^{6,7}

For the calculations in this paper, we used a mixture of QM-based methods to investigate the isomerization reaction. For the reaction in the gas phase, in solution, and in a small model of the active site we employed pure QM approaches, whereas for the simulation of the reaction in the protein we resorted to hybrid QM/MM techniques. The

(6) Field, M. J. *The Simulation of Chemical Reactions*, in *Computer Simulation of Biomolecular Systems: Theoretical and Experimental Applications*; van Gunsteren, W. F., Weiner, P. K., Wilkinson, A. J., Eds.; ESCOM: Leiden, 1993; Vol. 2, pp 82–123.

(7) Gao, J. *Methods and Applications of Combined Quantum and Molecular Mechanical Potentials*. In *Reviews in Computational Chemistry*; Lipkowitz, K. B., Boyd, D. B., Eds.; VCH: New York, 1995; Vol. 7, pp 119–185.

gas- and solution-phase calculations were performed mainly to calibrate the methods to be employed for the studies in the enzyme. Our strategy is described in detail in the sections below.

Before continuing, we define some of the terms that we use in the rest of the paper. The isomerization reaction that we chose to study in this paper is normally that from deprotonated AHB to deprotonated HMOV, although we also consider the reaction from deprotonated AHB to protonated HMOV in the enzyme (see Figure 1 and steps b and c of Figure 2, respectively). We refer to the deprotonated AHB as the reactant form of the substrate, the deprotonated or protonated HMOV as the product form of the substrate, and reserve the term “substrate” to refer to the molecule undergoing the reaction, no matter which chemical state it happens to be in.

2.1. Gas-Phase and Implicit-Solvent Calculations. To map out the profile of the reaction in the gas phase, we performed semiempirical and ab initio QM calculations with the MOPAC⁸ and Jaguar⁹ programs, respectively. The structures of the reactant and product were built de novo and their geometries optimized using the appropriate minimizers in the program packages. Likewise, the saddle-point structures were optimized using a mode-walking algorithm (in MOPAC) or by starting from the MOPAC-optimized structure (in Jaguar). A harmonic frequency analysis was performed on all optimized structures so that the

(8) Stewart, J. J. P. *Mopac 7.0*, QCPE 688; Quantum Chemistry Program Exchange: Bloomington, IN, 1993.

(9) *Jaguar 3.5*; Schrödinger Inc.: Portland, OR, 1998.

nature of the stationary points could be characterized. For the semiempirical calculations both the AM1¹⁰ and PM3^{11,12} Hamiltonians were tried, whereas *ab initio* calculations were performed at the Hartree-Fock (HF) and the density functional theory (DFT)/B3LYP¹³ levels with the 6-311G**+ basis set.¹⁴

To obtain an idea of the effect of aqueous solution on the reaction profile, the calculations in the gas phase were repeated but this time with implicit models of solvent. The methods used were the AM1-SM1 and PM3-SM3 models implemented in the AMPAC program,¹⁵ the AM1-COSMO and PM3-COSMO models found in MOPAC, and the self-consistent reaction field method of Jaguar. In each case, a dielectric constant appropriate to that of water at 300 K was employed.

2.2. Semiempirical Hybrid-Potential Calculations. The calculations of section 2.1 were pure QM calculations in which the reaction profiles were obtained by geometry optimization techniques. While the calculation of reaction paths using minimization-type approaches is useful, it is the free energy that is the quantity of primary interest when investigating reaction processes. Thus, in our semiempirical hybrid potential calculations we have preferred to calculate the free-energy profiles using the method of umbrella sampling. In this section we first describe the models we used before detailing how we carried out the free-energy calculations.

All the calculations in this section were performed with the DYNAMO molecular modeling program^{16,17} which has been developed in our laboratory for hybrid potential simulations. The implementation of the hybrid potential is essentially similar to that of ref 18 and is fully explained in ref 17. We chose the AM1 method with the magnesium parameters of Hutter et al.¹⁹ to treat the QM atoms as our tests showed that the PM3 method performed poorly when the magnesium atoms were treated quantum mechanically. For the atoms of the MM region, the all-atom OPLS force field was employed²⁰ with the TIP3P model of water.²¹

2.2.1. Explicit-Solvent Calculations. To have a direct comparison with the results of the implicit-solvent model QM calculations, we performed our first hybrid potential calculation for the isomerization reaction in water. To do this, we took the substrate which was treated quantum mechanically and immersed it in a box of 729 MM waters. All water molecules which overlapped with the substrate or were within 2.8 Å of it were then deleted, and the complete system was subjected to a short dynamics simulation. The process of superposition and dynamics simulation was repeated until no more water molecules could be added. After this the system was subjected to a final simulation of 10 ps duration to fully equilibrate it in preparation for the free-energy calculations.

2.2.2. Enzyme Calculations. We shall present results for six enzyme/substrate models that we studied and which we denote F18, F52, F52p, F63p, R18, and R52. The models R18 and R52 (R = "reduced") were built around a 52-atom model of the active site/substrate complex, whereas the remaining models (F = "full") contained all the atoms of the surrounding protein and solvent. The numbers 18, 52, and 63 in the notation refer to the numbers of atoms in their QM regions, and

the "p" indicates that the side-chain carboxylate group of residue Glu 496 is protonated.

The reduced 52-atom models of the active site were built from the X-ray structure. The basic model consisted of the substrate which was built from the IpOHA inhibitor, the two magnesium cations, the five water molecules detected in the active site of the X-ray structure, and the side chains of the residues Asp 315 and Glu 319 that help stabilize the magnesiums. The side chains of the amino acids were cut between the C α and C β atoms, and the bonds broken by removal of the C α atoms were satisfied by the addition of hydrogen atoms at appropriate positions. All the atoms were left to move freely in the simulations except for the terminal methyl groups of the broken amino acid side chains, whose coordinates were fixed in their crystallographic positions. In the R52 model all atoms in the model were treated quantum mechanically, whereas in the R18 model only the atoms of the substrate were in the QM region, the remaining atoms being treated with the MM force field. Construction of the models was followed by short geometry optimizations to remove any unfavorable energetic contacts.

The full models of the substrate-enzyme system were built from the X-ray structure of the protein/inhibitor complex determined by Biou et al.⁵ and published in the Protein Data Bank²² with the code 1YVE. The native protein is a dimer, but monomeric mutants of the protein, which have been prevented from dimerizing, exist and show catalytic activity.²³ Because of this and because the mutations are in loop regions that are far from the active sites, we chose to work on the monomer form of the protein so as to reduce the size of our model system. After extraction of the monomer we removed all water molecules present in the crystallographic structure except for the five molecules located in the active site, added the hydrogens to the protein using the molecular graphics program INSIGHT II,²⁴ and modeled the substrate from the IpOHA inhibitor. To solvate the structure a water sphere of 32 Å radius centered on the O3 oxygen of the substrate was superimposed upon the enzyme, and water molecules whose distance to the protein was inferior to 2.8 Å were deleted. This superposition was followed by a short molecular dynamics simulation to remove unfavorable energetic contacts, and the whole process of superposition and dynamics simulation was repeated until no more water molecules could be added. The final system consisted of 14 197 atoms. To reduce computational cost in our simulations, the positions of all atoms farther than 16.5 Å away from the O3 oxygen atom of the substrate were fixed; note that although the positions of these atoms were fixed, their interactions with the unfixed MM and QM atoms of the central region were still included.

In the F18 model only the 18 substrate atoms were treated quantum mechanically, and all the remaining atoms were treated molecular mechanically. In the F52 model the same atoms were treated quantum mechanically as in the R52 model, i.e., the substrate, the magnesium cations, five water molecules, and the side chains of the residues Asp 315 and Glu 319, broken between the C α and C β atoms. The F52p model was the same as the F52 model except that the side chain of Glu 496, which was in the MM region, was protonated. The F63p model was the same as the F52p model except that the protonated side chain of Glu 496, up to the C β atom, was put into the QM region. To satisfy the broken bonds between the QM and MM atoms, the link-atom approximation was used¹⁷ which requires adding extra "link" atoms (hydrogens), one for each broken bond, to the QM region. Each link atom is placed at 1.1 Å from the C β atom of the corresponding side chain in the direction of the C α atom. The QM regions for all the models are shown schematically in Figure 3. Construction of all models was terminated by carrying out a molecular dynamics simulation of 10 ps duration, and it was these structures which were used as the starting points for the free-energy calculations.

2.2.3. Free-Energy Calculations. To determine the free-energy profiles for the isomerization reaction, we calculated the potentials of mean force (PMF)²⁵ using the method of umbrella sampling.^{26,27} To do this, we employed the following strategy:

(22) Bernstein, F. C.; Koetzle, T. F.; Williams, G. J. B.; Meyer, E. F., Jr.; Brice, M. D.; Rodgers, J. R.; Kennard, O.; Shimanouchi, T.; Tasumi, M. *J. Mol. Biol.* **1977**, *112*, 535–542.

(23) Wessel, P.; Biou, V.; Douce, R.; Dumas, R. *Biochemistry* **1998**, *37*, 12753–12760.

(24) *Insight II*; Molecular Simulations Inc.: San Diego, CA, 1993.

(25) Kirkwood, J. G. *J. Chem. Phys.* **1935**, *3*, 300–313.

(10) Dewar, M. J. S.; Zoebisch, E. G.; Healy, E. F.; Stewart, J. J. P. *J. Am. Chem. Soc.* **1985**, *107*, 3902–3909.

(11) Stewart, J. J. P. *J. Comput. Chem.* **1989**, *10*, 209–220.

(12) Stewart, J. J. P. *J. Comput. Chem.* **1989**, *10*, 221–264.

(13) Becke, A. D. *J. Chem. Phys.* **1993**, *98*, 1372–77; **1993**, *98*, 5648–5652.

(14) Hehre, W. J.; Ratom, L.; Schleyer, P. v. R.; Pople, J. A. *Ab Initio Molecular Orbital Theory*; J. Wiley & Sons: New York, 1986.

(15) *AMPAC-5.0 Manual*; Semichem, 12715, W. 66th Terrace, Shawnee, KS 66216; 1994.

(16) Field, M. J. *A Practical Introduction to the Simulation of Molecular Systems*; Cambridge University Press: Cambridge, UK, 1999.

(17) Field, M. J.; Albe, M.; Bret, C.; Proust-de Martin, F.; Thomas, A. *J. Comput. Chem.* **2000**, *21*, 1088–1100.

(18) Field, M. J.; Bash, P. A.; Karplus, M. *J. Comput. Chem.* **1990**, *11*, 700–733.

(19) Hutter, M. C.; Reimers, J. R.; Hush, N. S. *J. Phys. Chem. B* **1998**, *102*, 8080–8090.

(20) Jorgensen, W. L.; Maxwell, D. S.; Tirado-Rives, J. *J. Am. Chem. Soc.* **1996**, *118*, 11225–11236.

(21) Jorgensen, W. L.; Chandrasekar, J.; Madura, J. D.; Impey, R. W.; Klein, M. L. *J. Chem. Phys.* **1983**, *79*, 926–935.

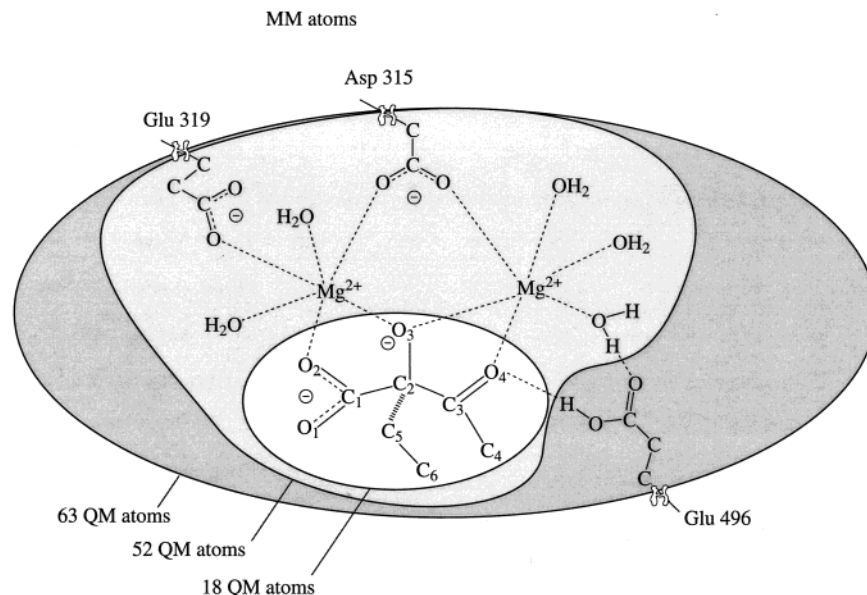


Figure 3. Schematic diagram of the quantum atoms in the three active site models employed for the QM and hybrid potential simulations. Note that in two of the six models, residue Glu 496 is protonated, whereas in the others it is deprotonated.

(1) Choose a reaction coordinate as a function of one or more coordinates, ξ_1, ξ_2, \dots , in the system. For the case of the isomerization, the results of the calculations in the gas phase and in solution and of tests in the enzyme showed that the mechanism of the reaction could be well described by a single coordinate consisting of the difference of the distances between the C2 and C5 and the C3 and C5 atoms of the substrate. Denoting these distances as d_{25} and d_{35} , respectively, the reaction coordinate is $d_{25} - d_{35}$. To test the validity of this single reaction coordinate we also calculated two-dimensional free-energy profiles in which the distances d_{25} and d_{35} were treated as separate variables.

We also investigated the proton transfer between the substrate and Glu 496 in the model F63p and for these free-energy calculations chose as the relevant coordinate the distance between the proton and the atom O4 of the substrate. We denote this coordinate as d_{OH} .

(2) Define umbrella potentials, v_i , for each of the coordinates, ξ_i . In all cases we took a harmonic form:

$$v_i(\xi_i) = \frac{1}{2}k_i(\xi_i - \xi_i^0)^2 \quad (1)$$

where k_i is the force constant for the potential and ξ_i^0 is a constant reference value for the coordinate.

(3) Perform a series of molecular dynamics simulations for the system in the presence of the umbrella potentials. The simulations are the same except that they are performed with different reference values of the coordinates, ξ_i^0 , in the umbrella potentials. The aim is to have the simulations sample the complete range of values of the ξ_i for which a free-energy profile is required. For the free-energy profile to be reasonable, it is also necessary that simulations with neighboring umbrella potential reference values sample regions of the reaction coordinate that overlap to some extent. In practice, we found that using a force constant of $2000 \text{ kJ mol}^{-1} \text{ \AA}^{-2}$ for the umbrella potentials and reference values that differed by 0.05 \AA between windows was adequate. To obtain converged PMFs, it was necessary to run the simulations for each window for about 10 ps with at least 2–3 ps of equilibration.

(4) At each step of the data-collection phases of the simulations, save the actual values of the coordinates, ξ_i , on an external file.

Once the reaction-coordinate data were collected from the simulations, the reaction-coordinate distribution functions were determined for each window and then pieced together using the weighted histogram

analysis (WHAM) method.²⁸ The resulting “unbiased” distribution function, $\langle \rho(\xi_1, \dots) \rangle$, was then used to calculate the PMF, W , from

$$W(\xi_1, \dots) = c - k_B T \ln \langle \rho(\xi_1, \dots) \rangle \quad (2)$$

where k_B is Boltzmann’s constant, T is the temperature, and c is an arbitrary additive constant. As has been reported elsewhere,²⁹ we found the WHAM method to be a reliable way of extracting free-energy profiles in one or more dimensions.

All molecular dynamics simulations were done at a temperature of 300 K. A velocity–Verlet–Langevin algorithm was used with a friction coefficient of 10 ps^{-1} for each atom and a time step of 1 fs.³⁰ The QM/MM and MM/MM nonbonding interactions were calculated using an atom-based force-switching (ABFS) truncation function with inner and outer cutoffs of 9.5 and 13.5 Å, respectively,^{16,31} whereas all interactions were calculated without truncation in the purely QM R52 simulations. Tests showed that the ABFS truncation scheme combined with the cutoff criteria that we employed gave results essentially equivalent to those obtained using calculations in which there was no truncation.

All calculations were done on PC/Linux-based systems and up to 60 processors of a Cray T3E parallel machine at the CEA computer center in Grenoble. On the CRAY, 1 ps of dynamics of our simulation system with 52 atoms in the QM region took about 100 min on a single processor. All our free-energy calculations were perfectly parallelizable because the simulations for separate windows were run simultaneously and independently on separate processors.

2.2.4. Ab Initio Calculations. Although the semiempirical AM1 method gives good results in many circumstances, we wanted to test its reliability for the description of the reaction in our enzyme–substrate models by making comparisons with the results of more accurate ab initio QM calculations. Unfortunately, it is currently impractical to perform free-energy calculations directly with ab initio techniques for models of the size that we are considering.

Instead we adopted an approach in which we computed reaction paths for the model and the reaction that we wanted to test using minimization techniques and the semiempirical AM1 hybrid potential. We then compared the semiempirical QM energies for each of the

(28) Kumar, S.; Bouzida, D.; Swendsen, R. H.; Kollman, P. A.; Rosenberg, J. M. *J. Comput. Chem.* **1992**, *13*, 1011–1021.

(29) Roux, B. *Comput. Phys. Commun.* **1995**, *91*, 275–282.

(30) Allen, M. P.; Tildesley, D. J. *Computer Simulation of Liquids*; Oxford University Press: Oxford, UK, 1987.

(31) Steinbach, P. J.; Brooks, B. R. *J. Comput. Chem.* **1994**, *15*, 667–683.

(26) Valleau, J. P.; Torrie, G. M. A Guide for Monte Carlo for Statistical Mechanics. In *Statistical Mechanics*; Berne, B. J., Ed.; Plenum Press: New York, 1977; Part A, pp 169–194.

(27) Torrie, G. M.; Valleau, J. P. *Chem. Phys. Lett.* **1974**, *28*, 578–581.

Table 1. Relative Energies of the Optimized Substrate, Saddle Point, and Product Structures for the Isomerization Reaction in the Gas Phase^a

method	reactant	saddle point	product
AM1	0.0	56.2	-47.6
PM3	0.0	59.3	-52.7
HF	0.0	82.6	-45.1
DFT	0.0	33.5	-44.2
QCISD	0.0	50.8	-46.8

^a All structures were optimized at the relevant level of theory except for the QCISD calculations which used the DFT optimized geometries. The HF and DFT optimizations were done with a 6-311+G(d,p) basis set, while the QCISD calculations were performed with a 6-311G(d) basis. Energies are in kJ mol⁻¹.

structures along the path with the ab initio QM energies obtained using HF and DFT calculations on the same structures. The procedure that we used to calculate the paths was as follows:

(1) A starting structure was selected for the enzyme-substrate complex by taking a structure from one of the molecular dynamics trajectories generated during the free-energy calculations. Depending upon the model and the reaction we were studying, we normally started with a structure from near the top of the barrier of the appropriate free-energy profile.

(2) The structure was minimized with the semiempirical hybrid potential and with very strong harmonic constraints ($k_i \approx 20\,000$ kJ mol⁻¹ Å⁻² in eq 1) to keep the reaction coordinate variables close to their initial values.

(3) Starting from the minimized structure of step 2, new structures were obtained by both incrementing and decrementing the reference values of the reaction coordinates by 0.05 Å and then re-minimizing. This procedure was repeated until a series of minimized structures was obtained that spanned the complete range of the reaction path.

(4) The energies of each of the minimized structures along the pathway were obtained using ab initio HF and DFT calculations. The basis set and other details of the ab initio calculations were the same as those described in section 2.1. Note that the same numbers of QM atoms were treated in both the semiempirical and ab initio calculations and that the charges of the MM atoms were included in the ab initio QM calculations in the same way as they were in the semiempirical calculations.

3. Results

3.1. Gas-Phase Calculations. The relative energies of the intermediates and the saddle point in the gas phase at different levels of theory are presented in Table 1. For all the methods, the product is more stable than the reactant by about 45–50 kJ mol⁻¹, which can be rationalized by noting that the negatively charged groups are farther apart in the product than they are in the reactant. There is more variability with the saddle point energies: the semiempirical methods give barriers of about 60 kJ mol⁻¹, whereas the HF ab initio result is higher and the DFT result is lower. Given the well-known propensity of HF methods to overestimate barrier heights and the common observation that DFT methods often underestimate them, it is likely that the semiempirical result is a reasonable compromise value. However, to verify this assertion we performed higher-level correlated molecular orbital calculations at the B3LYP-optimized geometries using the Gaussian 98 program.³² Due to the computational demands of these calculations and our available computer resources, the best we could do were QCISD calculations with a 6-311G(d) basis set. The resulting values are shown in Table 1, where it can be seen that the results are in good agreement with the semiempirical calculations. In contrast to the energies, the structures are very similar with root-mean-square coordinate deviations of less than 0.15 Å between each of the structures within each category.

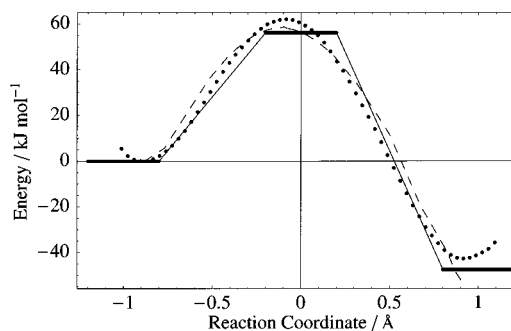


Figure 4. Energy profiles for the reaction in the gas-phase using the AM1 semiempirical method. The solid lines represent the energies of the optimized substrate, saddle point, and product structures; the dashed line represents the minimum-energy reaction path calculated between these structures; and the dotted line shows the free-energy profile obtained from an umbrella sampling calculation. The reaction coordinate is defined as $d_{25} - d_{35}$.

Once the stationary point structures are known, it is straightforward to determine the minimum-energy reaction path (MERP) between them and analyze the mechanism of the isomerization. Having done this, it was clear that the distances d_{25} and d_{35} were the coordinates that varied the most along the path and that, as d_{25} increased, d_{35} decreased by an equal amount. Thus, the linear combination of these distances $d_{25} - d_{35}$ represents a good single-coordinate description of the isomerization mechanism. The energy profile of the MERP plotted using this coordinate is shown in Figure 4. Also shown in the figure are the energy values of the stationary points and the free-energy profile that is obtained by performing an umbrella sampling calculation in the gas phase. The barrier height of the free-energy profile is similar to that of the MERP except that the position of the barrier is shifted slightly toward the reactant structure. The validity of the single-coordinate reaction path description can be seen from Figure 5, in which we have plotted the free-energy surface for the gas-phase reaction calculated as a function of the two distances d_{25} and d_{35} . It is obvious from this that no path of significantly lower energy can be found by using some other combination of the distances d_{25} and d_{35} .

3.2. Implicit- and Explicit-Solvent Calculations. The relative energies calculated using the implicit-solvent models are reported in Table 2. As with the gas-phase results, the energy values show some variability, depending upon the method, but certain trends are obvious. First, and in contrast to the case for the gas phase, the reactant structure is more stable in solvent than the product by about 40–50 kJ mol⁻¹. Second, the barrier to reaction on going from the reactant structure is about 3 times greater, 150 as opposed to 50 kJ mol⁻¹, whereas it is approximately the same on going from the product structure, at 100 kJ mol⁻¹. The extra stabilization of the reactant form of the substrate in solution can be understood because it has a dipole moment which is approximately twice as big as those of the saddle point and product forms, which themselves have

(32) Frisch, M. J.; Trucks, G. W.; Schlegel, H. B.; Scuseria, G. E.; Robb, M. A.; Cheeseman, J. R.; Zakrzewski, V. G.; Montgomery, J. A., Jr.; Stratmann, R. E.; Burant, J. C.; Dapprich, S.; Millam, J. M.; Daniels, A. D.; Kudin, K. N.; Strain, M. C.; Farkas, O.; Tomasi, J.; Barone, V.; Cossi, M.; Cammi, R.; Mennucci, B.; Pomelli, C.; Adamo, C.; Clifford, S.; Ochterski, J.; Petersson, G. A.; Ayala, P. Y.; Cui, Q.; Morokuma, K.; Malick, D. K.; Rabuck, A. D.; Raghavachari, K.; Foresman, J. B.; Cioslowski, J.; Ortiz, J. V.; Stefanov, B. B.; Liu, G.; Liashenko, A.; Piskorz, P.; Komaromi, I.; Gomperts, R.; Martin, R. L.; Fox, D. J.; Keith, T.; Al-Laham, M. A.; Peng, C. Y.; Nanayakkara, A.; Gonzalez, C.; Challacombe, M.; Gill, P. M. W.; Johnson, B. G.; Chen, W.; Wong, M. W.; Andres, J. L.; Head-Gordon, M.; Replogle, E. S.; Pople, J. A. *Gaussian 98*, Revision A.7; Gaussian, Inc.: Pittsburgh, PA, 1998.

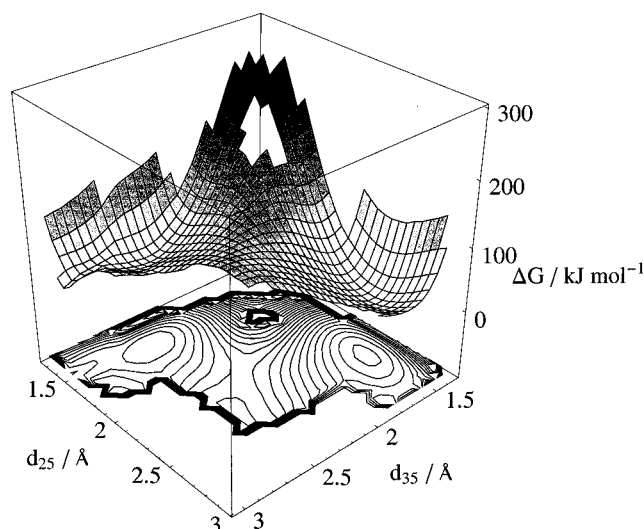


Figure 5. Free-energy surface for the gas-phase reaction calculated using the AM1 semiempirical Hamiltonian and an umbrella sampling method. The surface is calculated as a function of the distances d_{25} and d_{35} .

Table 2. Relative Energies of the Optimized Substrate, Saddle Point, and Product Structures for the Isomerization Reaction in Implicit Models of Solvent^a

method	reactant	saddle point	product
AM1-SM1	0.0	164.0	23.2
AM1-COSMO	0.0	148.6	53.1
PM3-SM3	0.0	121.3	31.7
PM3-COSMO	0.0	148.1	42.9
HF	0.0	187.4	67.6
DFT	0.0	132.8	58.5

^a Energies are in kJ mol^{-1} .

Table 3. Relative Free Energies of the Substrate, Transition-State, and Product Structures for the Isomerization Reaction in the Enzyme/Substrate Models in Which Residue Glu 496 Is Deprotonated^a

model	reactant	transition state	product
R18	0.0	181.4	69.3
R52	0.0	150.6	18.0
F18	0.0	208.8	113.4
F52	0.0	174.8	55.7

^a Energies are in kJ mol^{-1} .

dipole moments of similar magnitude. As in the gas phase, the barrier height predicted by the ab initio HF method is greater than the semiempirical values, whereas the DFT value is less.

The results obtained from the free-energy simulation with the explicit-solvent hybrid potential model can be compared to the implicit-solvent results as the latter estimate the free-energy of solvation. The explicit-solvent free-energy profile was determined as a function of the reaction coordinate $d_{25} - d_{35}$, but it will not be shown here because its shape is very similar to that of Figure 4. As with the implicit-solvent results, the reactant is more stable than the product, although the energy difference is much less pronounced, being only 4.0 kJ mol^{-1} . The barrier to the reaction is, however, more nearly similar, the explicit-solvent result being $139.3 \text{ kJ mol}^{-1}$.

3.3. Enzyme Calculations with Glu 496 Deprotonated. The relative free energies of the reactant, transition-state, and product structures determined using the four enzyme/substrate models with Glu 496 deprotonated are shown in Table 3. Note that when talking about free energies, it is no longer appropriate to talk about saddle point structures, and so we will use the alternative

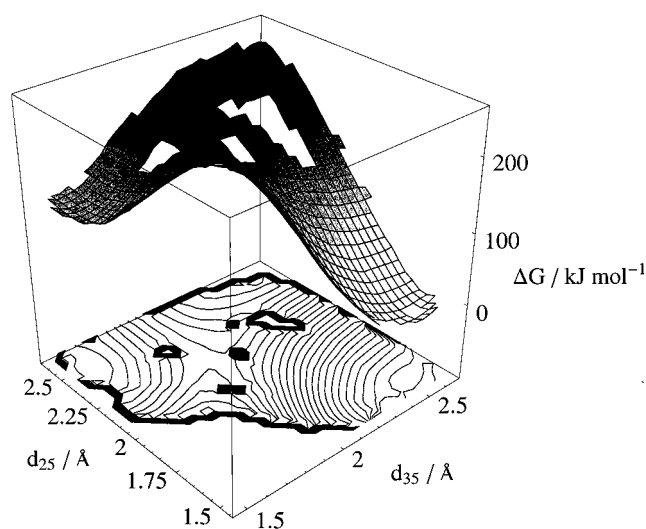


Figure 6. Free-energy surface for the F52 enzyme model as a function of the distances d_{25} and d_{35} .

term “transition state” instead. The results show a pattern similar to those in solution, with the product form of the substrate being less stable than the reactant form and the transition state being about 100 kJ mol^{-1} higher in energy than the product. The results for the most complete model, F52, are likely to be the most reliable, but it is instructive to compare the F52 energies with those of the other models. Two points stand out. First, the addition of protein atoms to the model ($\text{R18} \rightarrow \text{F18}$ and $\text{R52} \rightarrow \text{F52}$) increases the energies of both the transition state and product energies relative to the reactant. Second, the inclusion of a larger number of atoms, in particular the magnesiums, in the QM region ($\text{R18} \rightarrow \text{R52}$ and $\text{F18} \rightarrow \text{F52}$) counteracts this effect and decreases the energies of the transition state and product energies relative to that of the reactant.

While we do not show here the free-energy profiles for the reaction in each of the enzyme models, we do give in Figure 6 the full free-energy surface for the F52 model as a function of the distances d_{25} and d_{35} . This shows that the path of the reaction in the enzyme follows the same pattern as that in the gas phase and in solution with a single transition-state structure and that the path of lowest energy is well approximated by the difference in the distances $d_{25} - d_{35}$.

The height of the barrier to the isomerization determined from the free-energy calculations is $\sim 170 \text{ kJ mol}^{-1}$. Experimentally, it is known that AHIR has a very slow turnover ($k_{\text{cat}} = 6.3 \text{ s}^{-1}$ for the AHB substrate), and it has been proposed by Chunduru et al. that the alkyl migration is the rate-limiting step in the overall reaction.³³ D-Xylose isomerase, a similar magnesium-containing enzyme, also has a very low turnover ($k_{\text{cat}} = 1.0 \text{ s}^{-1}$). Recently, Wessel et al. determined experimentally the activation energy at 298 K for the overall reaction in the native dimeric protein and in a monomeric mutant and obtained values of 46 and 86 kJ mol^{-1} , respectively.²³

There are several reasons why the calculated barriers listed in Table 3 could be too high. To test whether the discrepancy is due to the AM1 method, we determined a reaction path for the F52 model reaction as described in section 2.2.4 and compared the AM1 and ab initio quantum mechanical energies for each structure along the path. The results are displayed in Figure 7. They show the same basic trends as the results in Tables 1 and 2 in that the DFT energies are lower than the AM1

(33) Chunduru, S. K.; Mrachko, G. T.; Calvo, K. C. *Biochemistry* **1989**, *28*, 486–493.

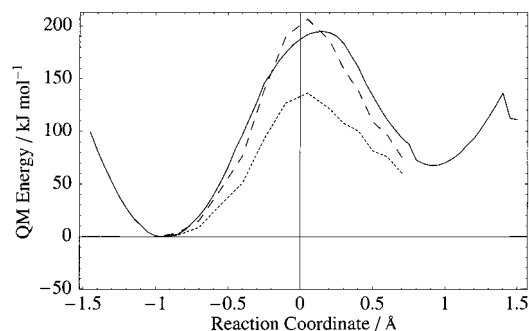


Figure 7. Comparison of the quantum mechanical potential energies for the F52 model using the semiempirical AM1 model (solid line), an ab initio Hartree-Fock approach (dashed line), and an ab initio DFT method (dotted line). Full details of how the calculations were performed are given in the text.

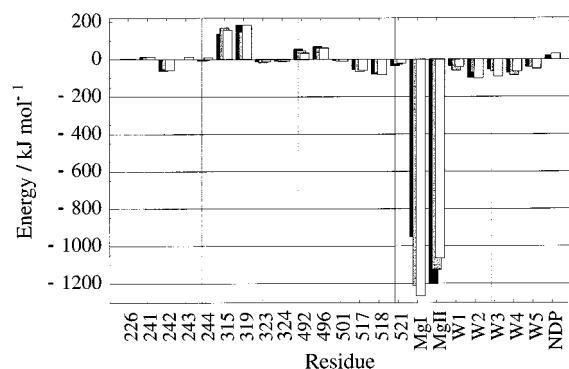


Figure 8. Histogram of the interaction energies between the reactant, transition-state, and product forms of the substrate and various groups in the enzyme system. The columns are, from top to bottom, for the reactant, transition state, and product. The numbers on the abscissa refer to the residues in the protein, MgI and MgII are the magnesium cations, W1–W5 are the water molecules in the active site, and NDP is the NADP. Energies are in kJ mol^{-1} .

results and the HF values are higher, albeit less so than for the results of the gas-phase and implicit-solvent calculations. The fact that the ab initio curves bracket the semiempirical ones in this way indicates that the semiempirical QM method is likely to describe the energetics of the reaction process in the enzyme as reliably as it does in the gas phase and in solution.

To obtain further insights into the source of the disagreement between our calculations and experiment, we decided to analyze in detail the interactions between the substrate and the magnesiums, the waters in the active site, and various residues of the protein using the F52 model of the enzyme/substrate system. This was done by performing three simulations each of 15 ps duration for the reactant, transition-state, and product forms of the substrate. The substrate was constrained to be of the correct form by performing the simulations with appropriate constraints on the value of the reaction coordinate variables. The interaction energies were calculated for structures at 0.1 ps intervals along each of the trajectories and then averaged over the full trajectory to obtain the final values. The interaction energies themselves were calculated using the DYNAMO implementation of the energy partitioning algorithm found in the MOPAC program.⁸ The interaction energies determined in this way are exact as, due to the approximations inherent in the AM1 method, the total quantum energy for the system can be exactly decomposed into two-body terms once the wave function has been determined.

The interaction energies are shown in Figure 8 for residues 226, 250–254, 315, 319, 523–524, 492, 496, 501, 517, 518,

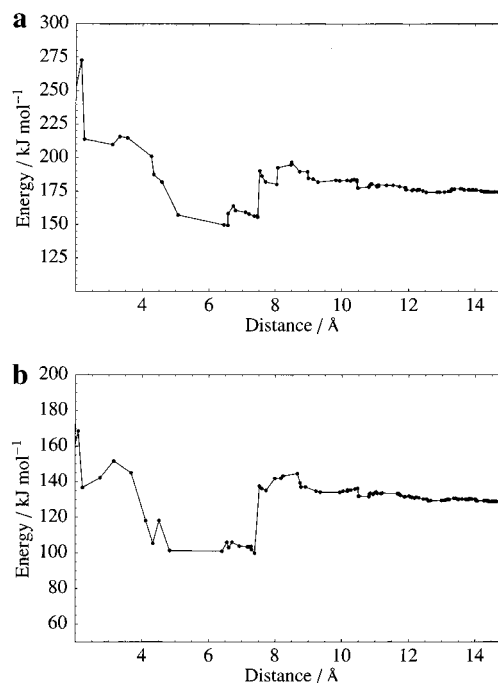


Figure 9. Difference in the cumulative interaction energies between (a) the transition-state and reactant and (b) the product and reactant forms of the substrate as a function of distance. The distances are determined between the O3 atom of the substrate and the center of mass of the relevant group of the enzyme system in the crystallographic structure.

and 521 of the protein, the two magnesiums, MgI and MgII, the five waters in the active site, W1, W2, W3, W4, and W5, and the nicotinamide. The most striking point about the figure is the large, stabilizing interaction that each of the magnesiums has on the three forms of the substrate and the variations in these energies between the three forms. Thus, the reactant is stabilized strongly by MgI, the product by MgII, and the transition state about equally by both magnesiums. The total interaction energy between the magnesiums and the substrate decreases along the reaction path, being largest for the reactant and lowest for the product.

All the other interaction energies are much smaller and have similar magnitudes for the reactant, transition state, and product. Residues Asp 315 and Glu 319 have the largest destabilizing interaction because they are negatively charged and close to the substrate, whereas all the waters, which are also close, stabilize the substrate. It should be noted that the primary role of residues Asp 315 and Glu 319 is to bind the magnesiums into the active site and that the destabilization caused by them will be more than compensated by the stabilizing effect of the magnesiums.

To show the distance dependence of the interaction energies we plot the differences between the cumulative enzyme/substrate interaction energies for the product and reactant and between those for the transition-state and reactant forms of the substrate as a function of distance in Figure 9a and b, respectively. From Figure 9a, it can be seen that the product is strongly destabilized relative to the reactant by the magnesiums at short distance, but that this effect is partially counteracted by the residues at longer range. The transition-state structure shows a similar behavior with respect to the reactant structure. There is an initial destabilization by the magnesiums and a subsequent partial restabilization by the residues farther away.

Notably in both Figure 9a and b, there is a destabilization at a distance of about 7.5 Å of both the product and the transition

state with respect to the reactant which, in each case, is caused by the residue, Glu 496. The reason for this destabilization is that the O4 oxygen of the substrate is at a relatively short distance ($\sim 3.5\text{--}4.0$ Å) from one of the oxygens of Glu 496, the other oxygen of Glu 496 being hydrogen-bonded to one of the water molecules that coordinates MgII. In the reactant form of the substrate O4 does not have a formal charge, but as the reaction proceeds the charge on the oxygen becomes greater and so the electrostatic repulsion between the oxygens becomes greater, thus causing the destabilization.

In all of our simulations the magnesium cations remain hexacoordinated and the average coordination structure shows only small changes as the isomerization reaction proceeds. The largest change occurs in the distance between MgII and the O3 atom of the substrate, which increases from 2.1 to 2.3 Å on going from reactant to product. In contrast, the MgII–O4 distance remains stable at about 2.1 Å. The movements around MgI are smaller, the largest being a decrease of 0.1 Å in the MgI–O3 distance as the reaction occurs. The distance between the magnesiums themselves increases during the reaction from about 3.5 to about 3.8 Å. These results are to be compared with the much larger movements observed for the magnesiums in the protein D-xylose isomerase,³⁴ which bears some similarities to AHIR.

3.4. Enzyme Calculations with Glu 496 Protonated.

Because of the results in the previous section, it is pertinent to ask how the free-energy profiles and the mechanism of the reaction would change if residue Glu 496 were protonated. To investigate this, we constructed a model F52p which was the same as the model F52 but with a proton on the “free” oxygen of Glu 496, the other oxygen being hydrogen-bonded to one of the water molecules coordinating MgII. Repeating the free-energy calculations with this model lowered the free-energy barrier a small amount to 158.6 kJ mol⁻¹ and decreased the energy difference between the reactant and product forms more substantially to 18.3 kJ mol⁻¹.

Of course, it is possible that the mechanism of the reaction changes if Glu 496 is protonated due to a coupling of the isomerization with a proton transfer from Glu 496 to the O4 atom of the substrate. The model F52p is an inappropriate one to test this hypothesis because the side chain of Glu 496 is included among the atoms of the MM region. Therefore, we constructed a sixth model, F63p, in which 11 atoms of the Glu 496 side chain were included in the QM region. As a first try, we redid the free-energy calculations for this model using the same variable $d_{25} - d_{35}$ as the reaction coordinate. The results we obtained were very similar to those of the model F52p with a barrier of 158.1 kJ mol⁻¹ and a reactant–product energy difference of 23.2 kJ mol⁻¹. An analysis of the trajectories generated during the molecular dynamics simulations showed that the proton remained bound to the oxygen of Glu 496 at all times and that there was a stable hydrogen bond between the proton and the substrate atom O4.

It was encouraging that the results for the F52p and F63p models were very similar, but we were suspicious about the stability of the protonated Glu 496 side chain, especially when it was hydrogen-bonded to the product form of the substrate. The reason for our doubts was the fact that the AM1 potential is known to overestimate the proton affinity of carboxylate anions (see, for example, refs 35 and 36). To validate the AM1 potential for this interaction, we adopted a procedure similar to

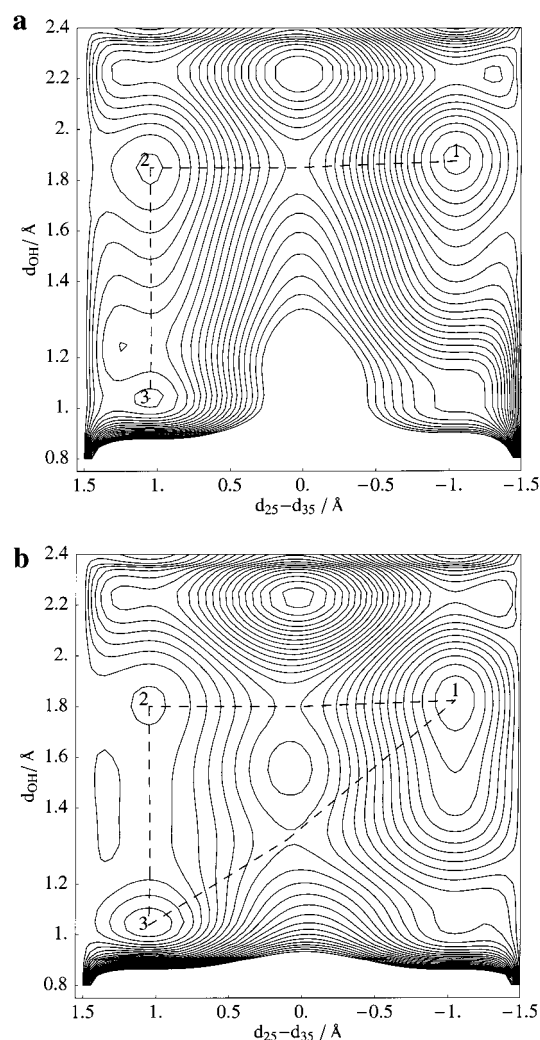


Figure 10. Contour maps of the minimum-energy reaction surfaces for the isomerization and proton-transfer processes: (a) for the AM1 hybrid potential and (b) the average of the DFT and HF ab initio surfaces. The reaction coordinate variables are $d_{25} - d_{35}$ and d_{OH} . Points 1, 2, and 3 refer to the reactant, deprotonated, and protonated product forms of the substrate, respectively. The dotted lines are for illustrative purposes only and only indicate approximately the lowest-energy paths. Energies are in kJ mol⁻¹ and distances in Å.

that described in section 2.2.4—that is, we generated a series of reaction paths for the isomerization process using the AM1 hybrid potential and a minimization technique for the F63p model. However, instead of generating a path as a function of just the variable $d_{25} - d_{35}$, we generated a reaction surface as a function of the two variables, $d_{25} - d_{35}$, and the proton–O4 substrate atom distance, d_{OH} . Corresponding surfaces were generated using the HF and DFT ab initio techniques and the same F63p QM/MM model. Plots of these surfaces are shown in Figure 10a and b. It is to be noted that while Figure 10a shows the surface obtained with the AM1 hybrid potential, Figure 10b shows an average of the surfaces obtained with the DFT and HF calculations. We did this because the topology of the surfaces at the DFT and HF levels of calculation were the same, the only difference being that the DFT surface was flatter than the HF surface. Also, as the DFT method often underestimates reaction barriers and the HF method overestimates them, we wanted some way of mixing the information from the two surfaces to correct for the deficiencies of each method. Although

(34) Hu, H.; Liu, H.; Shi, Y. *Proteins: Struct., Funct. Genet.* **1997**, *27*, 545–555.

(35) Dewar, M. J. S.; Dieter, K. M. *J. Am. Chem. Soc.* **1986**, *108*, 8075–8086.

(36) Thomas, A.; Jourand, D.; Bret, C.; Amara, P.; Field, M. J. *J. Am. Chem. Soc.* **1999**, *121*, 9693–9702.

we could have chosen different weights for performing the average, we thought that a simple average was the most unbiased choice in the absence of any other data.

It is clear from the figures that the two surfaces are qualitatively different. On the AM1 surface, the isomerization reaction occurs first with a barrier of about 180 kJ mol^{-1} and with the reactant form of the substrate being more stable than the deprotonated product form by about 50 kJ mol^{-1} . The proton-transfer process occurs afterward, with a barrier of approximately 50 kJ mol^{-1} , leading to a protonated product that is less stable than the deprotonated form by about 40 kJ mol^{-1} . On the ab initio surface, however, the preferred pathway is a concerted reaction in which the proton transfer occurs simultaneously with the isomerization. The barrier to the reaction is about 120 kJ mol^{-1} , and the protonated product is only about 50 kJ mol^{-1} less stable than the reactant form of the substrate. As on the AM1 surface, a stepwise mechanism is also possible, with the isomerization occurring first with a barrier of 130 kJ mol^{-1} , followed by the proton transfer with a very small barrier. In contrast to the AM1 results, though, the protonated form of the product is more stable than the deprotonated form by about 20 kJ mol^{-1} .

The surfaces in Figure 10 show potential energies, but we wanted to estimate the free energies to be consistent with our previous work. To do this we computed the free-energy surface for the isomerization and proton-transfer reactions as a function of the two variables $d_{25} - d_{35}$ and d_{OH} using our standard procedure and a "corrected" AM1 hybrid potential. The corrected hybrid potential, ν' , was the same as the normal one, ν , except that we added an extra term of the form

$$\nu' = \nu + E_{\text{AI}}(d_{25} - d_{35}, d_{\text{OH}}) - E_{\text{AM1}}(d_{25} - d_{35}, d_{\text{OH}}) \quad (3)$$

where E_{AI} and E_{AM1} are potential energies determined from the surfaces illustrated in Figure 10 and, as such, are functions of the variables $d_{25} - d_{35}$ and d_{OH} . The implementation of the corrected potential for use in a molecular dynamics simulation is straightforward. We did not attempt to fit the surfaces in any way but read in the tables of AM1 and ab initio energies defining the surface and then interpolated them using a two-dimensional spline technique³⁷ to obtain the values needed at each step of the simulation. The cost of calculating this extra term adds negligibly to the total time required for the calculation.

This method of correcting the AM1 potential is an approximation as it assumes that the structures defining the surface, determined by geometry optimizations with the AM1 hybrid potential, are representative of structures that would arise in a dynamics simulation with the same potential, and it also assumes that the AM1 structures are representative of those that would be obtained with an ab initio hybrid potential. Nevertheless, we feel that this way of correcting the energy is a useful one and can enable at least a semiquantitative estimate to be made of the free energies that would be obtained with an ab initio potential.

The free-energy surface determined with the corrected AM1 potential is displayed in Figure 11. It exhibits a behavior similar to that shown in Figure 10b. There are two possible pathways for the reaction: one in which the isomerization occurs before the proton transfer and one in which the two processes occur simultaneously. Both pathways have barriers with values of $\sim 110 \text{ kJ mol}^{-1}$ which are in reasonable accord with the experimental measurements. In contrast to the surfaces of Figure

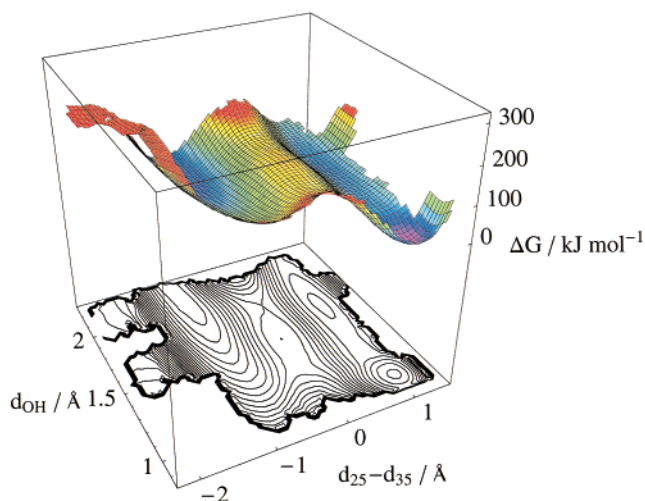


Figure 11. Free-energy surface for the isomerization and proton-transfer processes using the ab initio-corrected AM1 hybrid potential. The reaction coordinate variables are $d_{25} - d_{35}$ and d_{OH} . Energies are in kJ mol^{-1} and distances in \AA .

10, the protonated form of the product is more stable than both the unprotonated product and the reactant. These last two forms have approximately equal stability and are 30 kJ mol^{-1} less stable than the protonated product. The barrier to proton transfer from Glu 496 to the deprotonated product is small, with a value of less than 10 kJ mol^{-1} .

4. Conclusions

In this paper we have studied a possible mechanism for the isomerization step of the reaction catalyzed by the enzyme, AHIR. Our main conclusion is that the reaction appears to occur with the aid of a protonated Glu 496 residue, which stabilizes the transition state and product forms of the substrate by hydrogen-bonding to the negatively charged O4 atom. Our simulations also indicate that the proton transfer from Glu 496 to the substrate occurs almost simultaneously with the isomerization and so combines steps b and c of the proposed mechanism shown in Figure 2. Although its exact role may be open to doubt, the presence of Glu 496 is evidently important to the enzyme as it is conserved in all known plant AHIR sequences and homologous glutamate residues can be shown to exist in the equivalent bacterial enzymes.⁴

It is clear from an analysis of the enzyme/substrate binding that electrostatic interactions play the major role in the reaction and that the magnesiums are largely responsible for the electrostatic stabilization of the substrate. It is the interplay between the different ways in which the magnesiums interact with the substrate that largely determines the observed energy differences between the reactant, transition-state, and product forms of the substrate during the reaction.

The barriers to the isomerization process that we calculate are too high when compared to those measured experimentally, but we feel that the picture that we obtain is a plausible one and is also the best possible given the limitations of our models and the initial hypotheses that we made about the mechanism. The principal technical improvement that we could envisage to our approach is in the potentials that we employ to describe the reaction. In our opinion, however, it is unlikely that the barriers that we calculate can be substantially lowered. Other effects that could be important now that we have hypothesized that the isomerization reaction is coupled to a proton transfer

(37) Press, W. H.; Teukolsky, S. A.; Vetterling, W. T.; Flannery, B. P. *Numerical Recipes in Fortran: The Art of Scientific Computing*, 2nd ed.; Cambridge University Press: Cambridge, UK, 1992.

are quantum dynamical effects. Their influence would also lower the barrier, and their importance could be estimated by performing path-integral free-energy simulations similar to those discussed in refs 17 and 36.

It is also possible, of course, that the mechanism that we have hypothesized for the isomerization step is flawed. For example, it may be that the initial deprotonation of the substrate by a hydroxyl ion or a water molecule (step a in Figure 2) is concerted with the isomerization and reprotonation steps, or it may be that the reprotonation occurs with the aid of a water molecule rather than with Glu 496 (although we did not see this in our simulations). We are currently investigating some of these possibilities theoretically and also intend to mutate experimentally the protein to identify more precisely the role of Glu 496. The results of all these studies, along with those concerning other steps of the AHIR reaction and inhibitor design, will be reported in due course.

As a technical point, we would like to finish by pointing out that the method we describe in section 3.4 to correct the AM1 potential so that it more closely reproduces ab initio potentials should be of general use and can be fruitfully applied to the

simulation of other molecular systems. We think it has advantages over alternative approaches that reparametrize the AM1 or other semiempirical methods to obtain better agreement with experiment or ab initio data—first of all because it is easier to do and second because it is better controlled due to the fact that a reparametrization of a potential can inadvertently change its precision in other areas. We concede, however, that the approach is likely to be of most use when the calculated surfaces are functions of only a small number of degrees of freedom.

Acknowledgment. The authors thank Patricia Amara, Valerie Biou, Roland Douce, and Karine Thomazeau for help during the course of this work, the staff of the computer center at the CEA, Grenoble, for technical assistance, and a reviewer for helpful suggestions. Support was provided by the Institut de Biologie Structurale—Jean-Pierre Ebel, the Commissariat à l’Energie Atomique, the Centre National de la Recherche Scientifique, the Ministère de l’Education Nationale, de la Recherche et de la Technologie (decisions d’aide 98C0012 and 98C0013), and Rhône-Poulenc Agrochimie.

JA000414S